

Ultrafast B₁ mapping with RF-prepared 3D FLASH acquisition: Correcting the bias due to T₁-induced k-space filtering effect

Dan Zhu^{1,2}  | Michael Schär²  | Qin Qin^{1,2} 

¹F.M. Kirby Research Center for Functional Brain Imaging, Kennedy Krieger Institute, Baltimore, MD USA

²The Russell H. Morgan Department of Radiology and Radiological Science, Johns Hopkins University School of Medicine, Baltimore, MD USA

Correspondence

Dan Zhu, PhD,
F.M. Kirby Research Center for Functional Brain Imaging, Kennedy Krieger Institute, 716 N Broadway, Baltimore, MD 21205, USA.
Email: dzhu12@jhmi.edu

Funding information

Intellectual and Developmental Disabilities Research Center, Grant/Award Number: P50 HD103538; National Institutes of Health, Grant/Award Numbers: P41 EB031771, R01 HL135500, R01 HL138182, R01 HL144751

Purpose: The traditional radiofrequency (RF)-prepared B₁ mapping technique consists of one scan with an RF preparation module for flip angle-encoding and a second scan without this module for normalizing. To reduce the T₁-induced k-space filtering effect, this method is limited to 2D FLASH acquisition with a two-parameter method. A novel 3D RF-prepared three-parameter method for ultrafast B₁-mapping is proposed to correct the T₁-induced quantification bias.

Theory: The point spread function analysis of FLASH shows that the prepared longitudinal magnetization before the FLASH acquisition and the image signal obeys a linear (not proportional) relationship. The intercept of the linear function causes the quantification bias and can be captured by a third saturated scan.

Methods: Using the 2D double-angle method (DAM) as the reference, a 3D RF-prepared three-parameter protocol with 9 s duration was compared with the two-parameter method, as well as the saturated DAM (SDAM) method, the dual refocusing echo acquisition mode (DREAM) method, and the actual flip-angle imaging (AFI) method, for B₁ mapping of brain, breast, and abdomen with different orientations and shim settings at 3T.

Results: The 3D RF-prepared three-parameter method with complex-subtraction delivered consistently lower RMS error, error mean, error standard deviation, and higher concordance correlation coefficients values than the two-parameter method, the three-parameter method with magnitude-subtraction, the multi-slice DREAM and the 3D AFI, and were close to the results of 2D or multi-slice SDAM.

Conclusion: The proposed ultrafast 3D RF-prepared three-parameter method with complex-subtraction was demonstrated with high accuracy for B₁ mapping of brain, breast, and abdomen.

KEYWORDS

3D FLASH, B₁ mapping, complex-subtraction, k-space filtering effect, point spread function, RF-prepared B₁ mapping

1 | INTRODUCTION

Due to the proximity between the shorter radiofrequency (RF) wavelength at higher field strength and the size of the tissue, the homogeneity of the transmit RF field (B_1^+) is affected by both tissue composition and body geometry.^{1,2} Rapid measurement of the spatial variation of the flip angles (FAs) for the organs of interest is desired for many MRI applications, including subject-adaptive RF shimming using multiple RF transmission channels,³⁻⁷ FA correction for steady-state based T_1 ⁸⁻¹⁰ or T_2 ¹¹ measurement and spectroscopy-based metabolite quantification,¹²⁻¹⁴ determining the electric properties of the tissue or the local specific absorption rate (SAR) distribution,¹⁵⁻²² or evaluating the sensitivity to B_1^+ field inhomogeneities for novel pulse sequences.²³⁻³³

A number of B_1^+ mapping approaches have been commercialized by vendors. The conventional double-angle method (DAM), by taking the ratio of two images with excitation $FA = [\alpha, 2\alpha]$ for gradient echo or excitation/refocusing $FA = [\alpha/2\alpha, 2\alpha/4\alpha]$ for spin echo acquisitions,³⁴⁻³⁹ Requires $TR \gg T_1$ in order to remove the T_1 effect, thus is very time-consuming. The saturated double-angle method (SDAM)^{40,41} alleviated this TR restriction by inserting a B_1 -insensitive saturation module with a fixed saturation delay. Both DAM and SDAM are based on multi-slice 2D imaging, which is affected by imperfect slice profiles due to RF pulse shapes or B_0 inhomogeneities.³⁹ To avoid the dependence of the excitation profile across each slice, the so-called actual flip-angle imaging (AFI) method⁴² uses 3D fast gradient echo acquisition in pulsed steady-state with two interleaved TRs and the same FA. In contrast to these magnitude-based techniques, a phase-based method uses the Bloch-Siegert shift to encode the B_1 information.⁴³ Both AFI and Bloch-Siegert methods are still rather slow, taking minutes to cover a large volume. To speed up the imaging time to seconds, the dual refocusing echo acquisition mode (DREAM) method⁴⁴⁻⁴⁷ applies a STEAM preparation including two RF pulses followed by a 2D FLASH acquisition to obtain B_1 information in a single shot.

A more straightforward scheme is to apply a simple preparation module with only a single RF pulse for FA-encoding before the 2D FLASH⁴⁸ or 2D fast spin echo¹¹ acquisition (termed as RF-prepared method). One of the RF-prepared methods acquires two scans in a relatively short time, which starts with a B_1 -insensitive saturation module and a fixed saturation delay to remove the T_1 dependence as applied in SDAM, and precedes a 2D FLASH readout with the RF preparation module (for FA-encoding) in one scan and without this module (for normalizing) in another scan.^{49,50} Thus this last method eliminates any potential mismatch of RF profiles of two FAs in the presence of chemical shift (such as fat) or

B_0 inhomogeneity potentially faced by DAM or SDAM methods. Furthermore, by having separate preparation, the acquisition can be designed more flexibly.

In this work, we present a novel RF-prepared approach by using 3D FLASH acquisition with a long echo train duration for ultrafast B_1 mapping. A third scan is added with the saturation module immediately followed by the same readout, in order to record the bias from the k-space filtering effect induced by the T_1 relaxation during the long echo train. This bias needs to be subtracted from the first two images. We describe the theory in more detail below and compare the 3D RF-prepared method with a number of 2D or 3D methods for B_1 mapping of brain, breast, and abdomen with different shim settings at 3T. 2D DAM was chosen as the reference method for brain and breast, while 2D SDAM was chosen as the reference for abdomen due to limited scan time within a single breath-hold.

2 | METHODS

2.1 | Theory

The diagram of the proposed protocol is illustrated in Figure 1. The first two scans for FA-encoding and normalizing are conducted as in a typical RF-prepared method.^{49,50} The FA can be derived from the ratio of the longitudinal magnetization after an RF-prep pulse with $FA = \alpha$, M_{FA} , and the normalizing magnetization without this RF-prep pulse, M_{norm} :

$$\frac{M_{FA}}{M_{norm}} = \frac{M_{norm} \cdot \cos(\alpha)}{M_{norm}} = \cos(\alpha). \quad (1)$$

As done in SDAM,^{40,41} a B_1 -insensitive saturation module is used to establish M_{norm} after saturation recovery during a fixed delay.

With a two-parameter method, it is assumed that the acquired signal via a FLASH readout (S_{FA} and S_{norm}) are proportional to the prepared magnetizations, $S_{FA} = C \cdot M_{FA}$ and $S_{norm} = C \cdot M_{norm}$ where C is a constant determined by voxel sizes and coil specifications. Note that the signal evolution due to T_1 recovery through the FLASH acquisition leads to a k-space filtering effect (called partial saturation effect in the original paper⁴⁹), which is not proportional to the prepared magnetization. To keep this effect ignorable, the two-parameter method is limited to 2D acquisition with a short readout duration.

Based on our recent analysis of the point spread function (PSF) for FLASH acquisition,⁵¹ the signal modulation from this effect could be mainly characterized by the peak magnitude of the main lobe of the PSF(r), designated as PSF(0), where the spatial location $r = 0$ is the center of

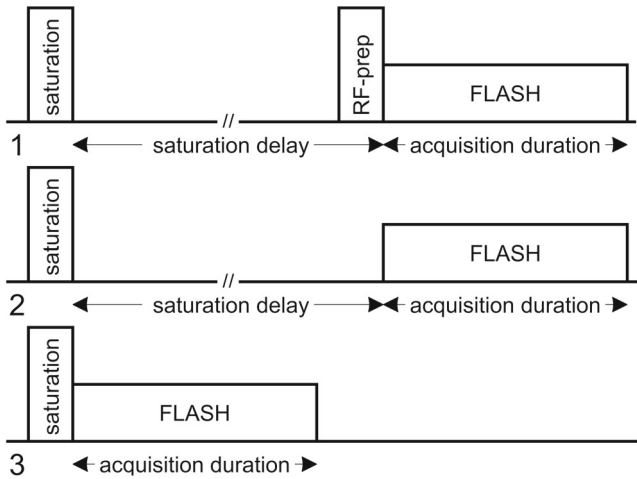


FIGURE 1 Pulse sequence of the 3D RF-prepared B_1 mapping technique, including three separate scans required for the proposed three-parameter method. A B_1 -insensitive saturation module followed by a fixed saturation delay is used to generate a consistent magnetization state for the first and the second scans. The same 3D FLASH acquisition with low-high profile ordering is applied for all three scans. In the first scan, an RF-prep module with a short hard pulse ($FA = \alpha$) is followed by a FLASH readout to generate an FA-encoded image. In the second scan, a normalizing image without applying the RF-prep module is acquired; In the third scan, the FLASH acquisition is applied immediately after the saturation module in order to obtain the imaging bias induced by the T_1 relaxation during the long readout

the symmetric spatial function. The signal intensity of a FLASH acquisition is proportional to $PSF(0)$, which is found to bear a linear relationship (Equation 29 in the PSF analysis paper⁵¹) with the initial longitudinal magnetization, M_{prep} :

$$S = C \cdot PSF(0) = C \cdot (a \cdot M_{prep} + b), \quad (2)$$

where a is a slope and b is the intercept (Equation 30 in the PSF analysis paper⁵¹).

Thus for the first two scans with arbitrarily long readout durations,

$$S_{norm} = C \cdot (a \cdot M_{norm} + b) \quad (3)$$

$$S_{FA} = C \cdot (a \cdot M_{norm} \cdot \cos(\alpha) + b). \quad (4)$$

As a result, the FA calculated with the traditional two-parameter method would lead to biased estimation.

In this work, we propose to obtain the intercept b via a third image, similar to the normalizing scan but without the saturation delay. Hence, the signal is acquired immediately after the longitudinal magnetization is fully saturated to 0 by the saturation module:

$$S_{sat} = C \cdot (a \cdot 0 + b) = C \cdot b. \quad (5)$$

Using a three-parameter method, the bias in FA estimation can thus be corrected:

$$\frac{S_{FA} - S_{sat}}{S_{norm} - S_{sat}} = \frac{C \cdot (a \cdot M_{norm} \cdot \cos(\alpha) + b) - C \cdot b}{C \cdot (a \cdot M_{norm} + b) - C \cdot b} = \cos(\alpha). \quad (6)$$

The relationship of the actual FA (α) and the nominal FA (α^{nom}) is usually described with a B_1^+ scale factor κ (with 100% as consistent between the two):

$$\kappa = \frac{\alpha}{\alpha^{nom}} \times 100\% = \frac{\arccos\left(\frac{S_{FA} - S_{sat}}{S_{norm} - S_{sat}}\right)}{\alpha^{nom}} \times 100\%. \quad (7)$$

It is important to note that, although the formulas above are based on the main lobe of the PSF, which implies that intercept b is a positive value, S_{sat} signal may be affected by the side lobes of PSF of surrounding pixels as well, which could have negative b values (Figure 4 in the PSF analysis paper⁵¹). Thus, subtractions between S_{FA} , S_{norm} and S_{sat} should consider opposite polarities and complex-subtraction is preferred in this case. Using complex values also avoids errors in B_1^+ estimation when $\alpha > 90^\circ$.

2.2 | Experiments

In vivo datasets of three brains, three breasts, and five abdomens were obtained from six volunteers (four females, two males; 25–45 y old). The study was approved by the Johns Hopkins School of Medicine Institutional Review Board and all subjects provided informed consent. Experiments were conducted on a 3T scanner (Ingenia; Philips Healthcare, Best, The Netherlands), with the body coil (maximum amplitude 13.5 μ T) equipped with a dual-source parallel RF excitation system.⁶ The maximum strength of the gradient coil was 40 mT/m and the maximum slew rate was 200 mT/m/ms. A 32-channel head coil, a 16-channel bilateral breast coil, and a 16-channel anterior torso coil combined with the 12-channel posterior coil under the table were used for signal reception in brain, breast, and abdomen scans, respectively.

For the three-parameter method (Figure 1), the RF-prep module for the FA-encoding scan used a 0.29 ms non-selective hard pulse with $\alpha^{nom} = 60^\circ$ immediately followed by spoiler gradients to dephase any residual transversal magnetization. All three scans applied a common saturation magnetization, which used a B_1 -insensitive WET pre-pulse⁵² consisting of four pulses with different FAs: 72° , 92° , 126° , and 193° interspersed with crusher gradients to null transversal magnetization.

The FLASH acquisition had a low-high profile ordering with the center of the k-space acquired at the beginning of the readout, and the specific parameters for brain scans were: TR/TE = 3.4/2.3 ms, FOV = $220 \times 220 \times 120 \text{ mm}^3$, imaging matrix = $56 \times 56 \times 30$, acquisition and reconstruction resolution = $4 \times 4 \times 4 \text{ mm}^3$, readout bandwidth (BW) = 2975 Hz/pixel, acceleration factor = 3 using the vendor-provided “Compressed-SENSE (CS)” technology. To investigate the effect of acquisition duration and saturation delay, the numbers of k-lines per shot were varied, [25, 50, 100, 225, 450], to have a different number of shots, [1, 2, 6, 12, 24]. With TR of 3.4 ms, the subsequent acquisition durations per shot were [86, 172, 343, 771, 1542] ms. For each acquisition scheme, corresponding acquisition FAs of [18°, 13°, 9°, 6°, 5°] were chosen for optimal signal contrast per unit time based on the PSF analysis for FLASH⁵¹ using a typical gray matter T_1 (1400 ms). Different saturation delays of [0.5, 1.0, 3.0] s were evaluated for all these scans while additional [0.75, 2.0, 5.0, 10.0, 20.0] s were added for the double- and single-shot scans. For the proposed three-parameter method with a single-shot acquisition (450 k-lines per shot, 1.54 s acquisition duration) and 2.0 s saturation delay (no saturation delay used in the third image), the total scan time was only 8.6 s.

Five other existing B_1 mapping methods with matched FOV, resolution/slice thickness, and the same CS factor of 3 were implemented to compare with our 3D RF-prepared method in the brain.

1. Single-slice DAM (2D DAM) with 60°/120° excitation FA by 0.58 ms non-selective hard pulses and single-shot fast-spin-echo acquisition (echo space of 3.7 ms, slice-selective refocusing FA = 180°), low-high profile ordering, readout BW = 1691 Hz/pixel, TR = 20 s, total scan duration 40 s. For comparison with other methods with either 3D or multi-slice coverage, three separate scans were performed in three orthogonal orientations at the center of the slabs.
2. Single-slice SDAM (2D SDAM) with the same acquisition as used in DAM, the same saturation module chosen in the RF-prepared protocol with a saturation delay of 0.5 s, TR = 0.58 s, total scan duration = 1.2 s. Three separate scans were performed in three orthogonal orientations.
3. Multi-slice SDAM with 2D SDAM repeated for 30 slices, readout BW = 1583 Hz/pixel, TR = 17 s, total scan duration = 34 s.
4. Multi-slice DREAM with a single-shot 2D FLASH acquisition of 30 slices, low-high profile ordering, with TR/TE_{STE}/TE_{FID} = 4.5/1.7/2.3 ms (stimulated echo first), STEAM/FLASH FA = 60°/15° and their slice thickness ratio = 2, readout BW = 3382 Hz/pixel, saturation effects mitigated by scanning odd slices first

and then even slices with equal temporal spacings of 0.5 s and the acquisition time between neighboring slices = 8.5 s, total scan duration = 17 s.

5. AFI with 3D FLASH acquisition of 30 slices, TR₁/TR₂/TE = 20/100/4.6 ms, FA = 60°, readout BW = 435 Hz/pixel, with adequate RF and gradient spoiling, total scan duration = 148 s.

For breast and abdomen scans, the specific acquisition parameters of the RF-prepared protocol were: FOV = $350 \times 350 \times 180 \text{ mm}^3$, imaging matrix = $58 \times 58 \times 30$, acquisition and reconstruction resolution = $6 \times 6 \times 6 \text{ mm}^3$, readout bandwidth = 2854 Hz/pixel, CS acceleration factor = 3. The single-shot acquisition (450 k-lines per shot) and 2.0 s saturation delay was chosen from the brain scan results for its efficiency (total scan duration kept 8.6 s). For breast scans, the five other existing B_1 mapping methods were also evaluated respectively with matched acquisition FOV and resolution. For abdomen scans, each method was acquired during one breath-hold. As a result, the 2D DAM method was not applied for the abdomen scans as its 40 s scan time is not suitable for single breath-hold scans. The multi-slice SDAM was acquired with 15 slices of 12 mm slice thickness, total scan duration = 17 s. The 3D AFI was only acquired for 3 slices of 6 mm slice thickness, total scan duration = 15 s. Only the axial orientation was imaged for the 2D DAM scan on breast and the 2D SDAM scans on both breast and abdomen.

B_1 shimming with standard single-source RF excitation (“Fixed”) was used for all three organs. For breast and abdomen scans, a dual-source B_1 shimming (“Adaptive”) was also performed. A vendor-provided B_1 shimming method based on geometries of individual breasts (“SMART”) was also applied for breast scans.

2.3 | Data analysis

For the 3D RF-prepared method, both magnitude and complex images after CS reconstruction were recorded. B_1^+ scale maps of the proposed 3D RF-prepared three-parameter method were calculated with Equation (7) with both magnitude- and complex-subtractions between the FA-encoded, the normalizing images and the saturated image pixel by pixel. The two-parameter results (without subtracting the saturated image) were also calculated for comparison. Respective B_1 maps based on other B_1 methods were computed as well. No image filtering was performed for any B_1 maps. A mask for each B_1 map was manually drawn from respective raw images to only include brain, breast, and abdomen tissues and avoid partial volume effect with air, skin, or skull. Within the mask area, the B_1 maps

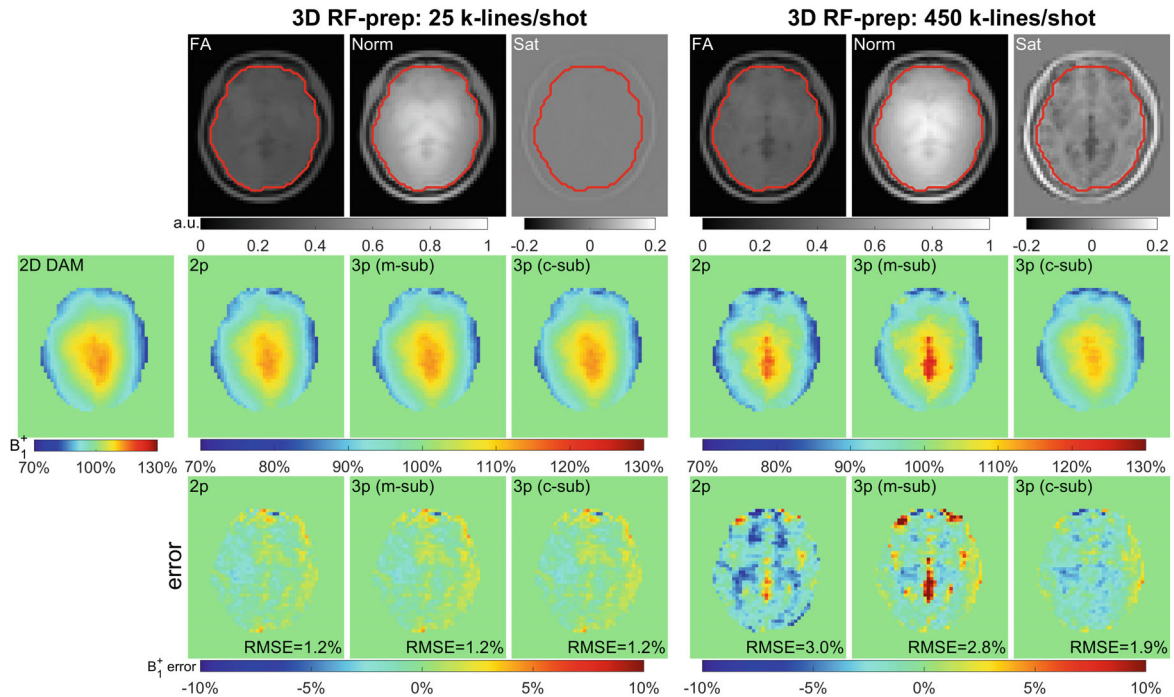


FIGURE 2 Evaluating the 3D RF-prepared B_1 mapping technique in the brain. (top): the FA-encoded, the normalizing, and the saturated images acquired with 25 and 450 k-lines per shot for 3D FLASH acquisition and a saturation delay of 3.0 s, with the tissue masks labeled in solid red lines; (middle): the calculated B_1^+ maps using the 2D DAM method, the RF-prepared two-parameter method, and the three-parameter method with both magnitude- and complex-subtractions; (bottom): their corresponding error maps (RF-prepared – DAM). RMSE of B_1^+ maps are labeled at the bottom of the corresponding error maps. FA: FA-encoded; Norm: normalizing; Sat: saturated; 2p: two-parameter method; 3p: three-parameter method; m-sub: magnitude-subtraction; c-sub: complex-subtraction

were quantitatively compared with the DAM (SDAM for abdomen scans) results using four metrics: (i) RMS error (RMSE), (ii) error mean, (iii) error standard deviation (SD), (iv) concordance correlation coefficients (CCC).

3 | RESULTS

The FA-encoded, normalizing and saturated images of an axial slice of a subject's brain, using 25 and 450 k-lines per shot for 3D FLASH acquisition and a saturation delay of 3.0 s, were shown in the first row of Figure 2. The calculated B_1 maps from the 2D DAM method, the 3D RF-prepared two-parameter method, and the proposed three-parameter method using both magnitude- and complex-subtraction methods are displayed in the second row of Figure 2. The third row exhibits the pixel-wise difference between the B_1 maps derived from 3D RF-prepared methods and 2D DAM method (RF-prepared – DAM). With only 25 k-lines per shot, the signal in the saturated image is rather small and the two- and three-parameter methods yielded similarly small errors (RMSE = 1.2%). When increasing to 450 k-lines per shot, the signal in the saturated image was higher and the two-parameter method generated higher errors (RMSE = 3.0%), which

was largely corrected via the three-parameter method with complex-subtraction (RMSE = 1.9%).

Figure 3 and Supporting Information Figure S1, which is available online arrays the B_1^+ scale maps of one axial slice of another subject's brain calculated from single-slice DAM, single-slice SDAM, multi-slice SDAM, DREAM, 3D AFI, and the 3D RF-prepared three-parameter method with complex-subtraction using different numbers of k-lines per shot with 3D FLASH acquisition and various saturation delays (where Figure 3 shows all saturation delays and Supporting Information Figure S1 shows all different numbers of k-lines per shot). All the results of the three-parameter method produced consistent B_1^+ scale distributions resembling five other methods (first row). The protocols with shorter saturation delays (less than 1 s) yielded lower SNR as expected. The single-shot acquisition (450 k-lines per shot) and 2.0 s saturation delay produced a good balance between B_1^+ mapping accuracy and the scan time (Supporting Information Figure S2), thus, were chosen as the recommended parameters and are the default setting for the three-parameter method mentioned below when not specified otherwise.

B_1^+ scale maps of three different brains using the 3D RF-prepared three-parameter method are displayed in axial, coronal, and sagittal orientations in Figure 4, with

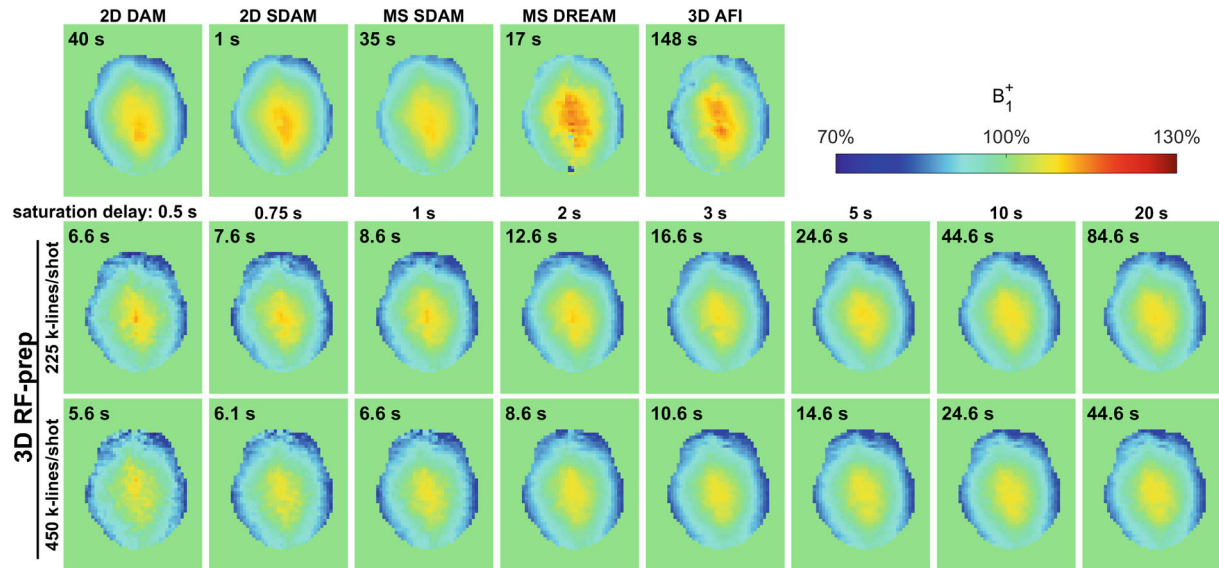


FIGURE 3 The brain B_1^+ maps of one axial slice calculated from 2D DAM, 2D SDAM, multi-slice (MS) SDAM, MS DREAM, 3D AFI, and the 3D RF-prepared three-parameter method with complex-subtraction using the double- and single-shot scans (225 and 450 k-lines per shot) with 3D FLASH acquisition and saturation delays of [0.5, 0.75, 1.0, 2.0, 3.0, 5.0, 10.0, 20.0] s. The total scan time for each method is labeled at each top left corner

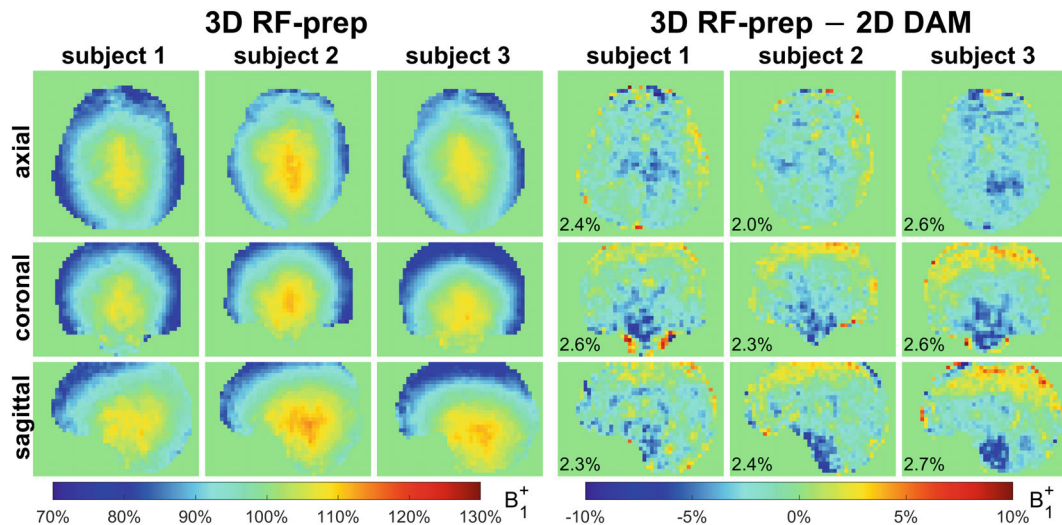


FIGURE 4 The brain B_1^+ maps of three subjects using the 3D RF-prepared three-parameter method in axial, coronal, and sagittal orientations and the corresponding difference maps when referenced to the 2D DAM results separately acquired in the three orientations (RF-prepared - DAM). RMSE values are labeled at the bottom of the difference maps

B_1^+ scales highest in the center of the cranium ($\sim 120\%$) reducing to lowest at the peripheral and superior of the brain ($\sim 80\%$). When using the results by 2D DAM separately acquired for each orientation as the reference, their small differences (RMSE = 2.0–2.7%) indicate consistent patterns between the two methods.

To exhibit the 3D-nature of the proposed method, B_1^+ scale maps in axial and sagittal orientations of three different breast at three different shimming conditions from the multi-slice SDAM method show consistent patterns

with the results from the corresponding reformed slices of the 3D three-parameter method in Figure 5, with the differences of B_1^+ scales between left and right breasts reduced from fixed shims to adaptive and SMART shims.⁵³ Supporting Information Figure S3 shows the results of an axial slice of a subject's breast with the calculated B_1^+ scale maps from the 2D DAM method, the 3D RF-prepared two-parameter method and the proposed three-parameter method using both magnitude- and complex-subtractions, and their respective difference

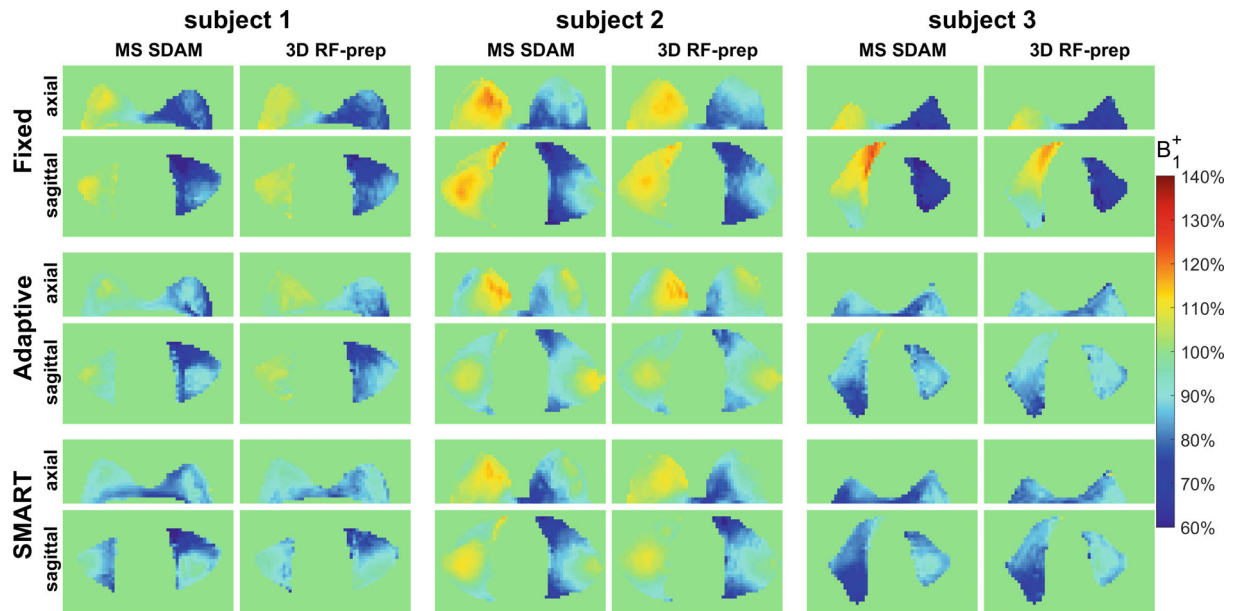


FIGURE 5 The breast B_1^+ maps of three subjects under fixed, adaptive, and SMART shims, respectively, from multi-slice SDAM method in axial and sagittal orientations and the 3D RF-prepared three-parameter method in the corresponding slices with consistent patterns

maps, under fixed, adaptive, and SMART shims respectively. Supporting Information Figure S4 arrays the B_1^+ scale maps of one axial slice of another subject's breast calculated from all six methods at three different shimming conditions.

Abdominal B_1^+ maps of three subjects at two different shimming conditions from the multi-slice SDAM method in axial and coronal orientations show consistent patterns with the results from the corresponding slices of the 3D three-parameter method in Figure 6, with the large B_1 shading effect under fixed shims mitigated under adaptive shims. Supporting Information Figure S5 shows the results of an axial slice of a subject's abdomen with the calculated B_1^+ scale maps from the 2D SDAM method, the 3D RF-prepared two-parameter method and the proposed three-parameter method using both magnitude and complex-subtractions, and their respective difference maps, under fixed and adaptive shims respectively. Supporting Information Figure S6 arrays the B_1^+ scale maps of one axial slice of another subject's abdomen calculated from five methods (DAM was not performed) at two different shimming conditions.

When combining comparison results from all three organs of all the subjects, including three orientations for each of the three brains, three shimming conditions for each of the three breasts, two shimming conditions for each of the five abdomens, the RMSE, error mean, error SD, and CCC values of each B_1 mapping method comparing to 2D DAM or SDAM methods for each organ are plotted in Figure 7 and Supporting Information Figure S7, S8, S9, respectively. Their averaged

values across 9 or 10 different data for each method and each organ are listed in Table 1. Compared to the 3D RF-prepared two-parameter method, the three-parameter method using complex-subtraction yielded the averaged RMSE 38% lower in the brain (2.4% vs. 3.9%), 45% lower in the breast (4.2% vs. 7.7%), and 27% lower in the abdomen (8.7% vs. 11.9%); it also had the averaged error mean values 37% lower in the brain (-1.2% vs. -1.9%), 68% lower in the breast (1.1% vs. -3.4%), and 85% lower in the abdomen (-1.1% vs. -7.3%); its CCC values were 5.9% higher in the brain (95.9% vs. 90.6%), 22% higher in the breast (83.0% vs. 68.1%), and 28% higher in the abdomen (68.2% vs. 53.1%) (Table 1). Note that the three-parameter method using magnitude-subtraction did not show such remarkable improvements (Figure 7, Table 1). Based on these quantitative metrics, the 3D RF-prepared three-parameter method with complex-subtraction delivered consistently lower RMSE, error mean, error SD, and higher CCC values than multi-slice DREAM and 3D AFI, and were close to the results of 2D or multi-slice SDAM (Figure 7, Table 1) but faster.

4 | DISCUSSION

The proposed three-parameter method enables the existing RF-prepared B_1^+ mapping technique to be extended to 3D FLASH long readout by correcting the T_1 -induced quantification bias enabling ultrafast volumetric B_1^+ mapping. The original paper⁴⁹ only recognized this k-space filtering effect and limited the acquisition to 2D FLASH

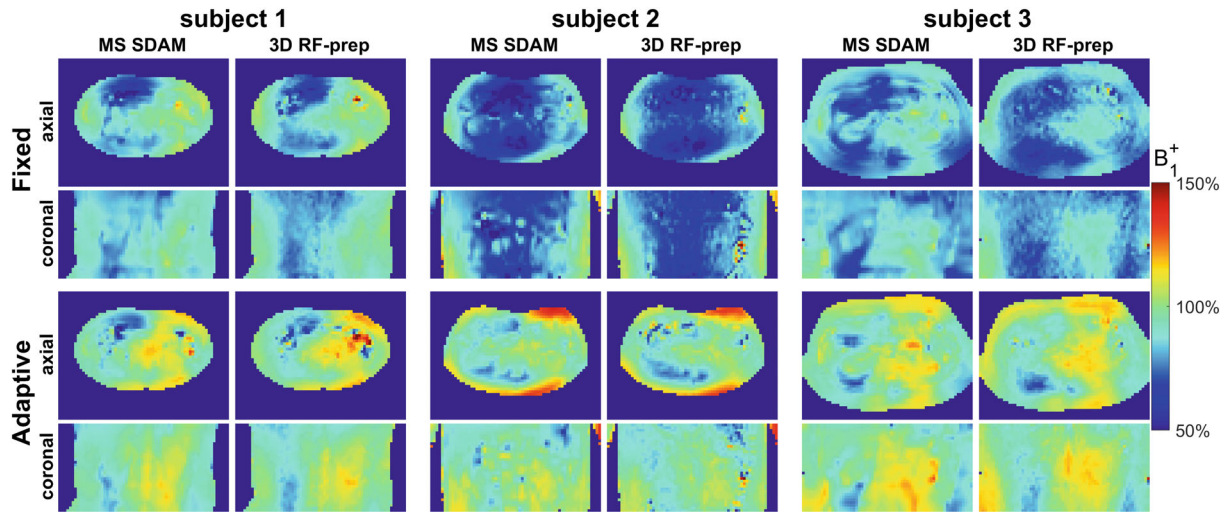


FIGURE 6 The abdomen B_1^+ maps of three subjects under fixed and adaptive shims, respectively, by the multi-slice SDAM method in axial and coronal orientations and the 3D RF-prepared three-parameter method in the corresponding slices with consistent patterns

acquisition so that this bias is negligible (Figure 2). The third saturated image added a very short extra time (1.54 s acquisition duration for the single-shot readout) and revealed this non-negligible bias. B_1^+ maps were more accurate when subtracting the saturated images from the FA-encoded and normalizing images respectively, than without this subtraction (Figure 2, Supporting Information Figures S3, S5). With the finding through PSF analysis of a linear (not proportional) relationship between the prepared longitudinal magnetization before the FLASH acquisition and the image signal (Equation 2), it became clear that the intercept of the linear function causes the quantification bias for the established two-parameter method. Both a higher number of k-lines per shot and a shorter T_1 value would lead to larger bias.⁵¹ Another character of the PSF of FLASH is its side lobes oscillating and phase-changing around zero. The tissue signal with a shorter T_1 (i.e., fat, white matter) could turn the surrounding tissue with low intensity due to its longer T_1 (i.e., CSF) to a negative signal. In this case, the magnitude-subtraction would amplify the quantification bias and the complex-subtraction indeed show better performance in different organs (Figures 2 and 7, Supporting Information Figures S3, S5, S7, S8, S9, Table 1).

Comprehensive comparisons between the proposed 3D RF-prepared method and five other established B_1 mapping techniques were performed in the brain, breast, and abdomen, respectively, for either different orientations or different shim conditions. Our method delivered similar performance as 2D or multi-slice SDAM, while taking only a quarter of the scan time of multi-slice SDAM with the same spatial coverage and resolution (8.6 s vs. 34 s). Compared to multi-slice DREAM, our method yielded largely

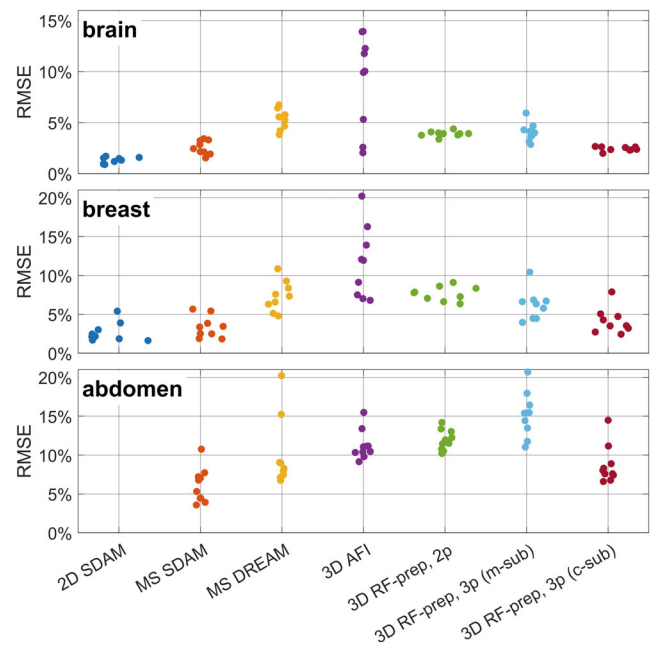


FIGURE 7 The swarm plot of the RMSE values of different B_1^+ mapping methods compared to 2D DAM or SDAM methods grouping three orientations for each of the three brains, three shimming conditions for each of three breasts, two shimming conditions for each of the five abdomens. Across three organs, RMSE of the 3D RF-prepared three-parameter (3p) method with complex-subtraction (c-sub) are consistently lower than the results of the two-parameter (2p) method or the 3p method with magnitude-subtraction (m-sub); RMSE of the 3D RF-prepared 3p method with c-sub are consistently lower than the results of 3D AFI and are close to the results of 2D or MS SDAM for all three organs, and are consistently lower than the results of MS DREAM in the brain and breast and are lower or close to in the abdomen

TABLE 1 RMSE, error mean, error SD, and CCC values of each B_1 mapping method compared to 2D DAM or SDAM methods averaged across three orientations for each of the three brains, three shimming conditions for each of three breasts, two shimming conditions for each of the five abdomens

		RMSE	Error mean	Error SD	CCC
Brain					
2D SDAM		1.3 ± 0.3	0.5 ± 0.6	1.1 ± 0.2	98.9 ± 0.4
MS SDAM		2.6 ± 0.7	1.6 ± 0.6	2.0 ± 0.5	95.5 ± 1.1
MS DREAM		5.3 ± 1.0	4.5 ± 0.8	2.7 ± 1.2	84.5 ± 5.1
3D AFI		9.1 ± 4.6	-3.3 ± 3.0	8.2 ± 4.1	69.1 ± 16.9
3D RF-Prep	2p	3.9 ± 0.3	-1.9 ± 1.0	3.2 ± 0.6	90.6 ± 2.1
	3p (m-sub)	4.1 ± 0.9	0.6 ± 1.2	3.9 ± 0.8	89.8 ± 3.5
	3p (c-sub)	2.4 ± 0.2	-1.2 ± 0.4	2.0 ± 0.4	95.9 ± 1.2
Breast					
2D SDAM		2.7 ± 1.2	-0.7 ± 0.6	2.5 ± 1.3	94.6 ± 4.8
MS SDAM		3.4 ± 1.4	0.2 ± 1.9	2.9 ± 1.3	91.5 ± 7.2
MS DREAM		7.4 ± 1.9	6.6 ± 1.9	3.0 ± 1.4	71.6 ± 19.3
3D AFI		11.6 ± 4.6	4.3 ± 3.1	10.2 ± 5.0	54.0 ± 29.8
3D RF-Prep	2p	7.7 ± 0.9	-3.4 ± 1.3	6.8 ± 0.9	68.1 ± 23.6
	3p (m-sub)	6.2 ± 1.9	3.9 ± 1.1	4.8 ± 1.6	76.1 ± 20.1
	3p (m-sub)	4.2 ± 1.6	1.1 ± 1.4	3.8 ± 1.6	83.0 ± 17.3
Abdomen					
MS SDAM		6.1 ± 2.2	-0.8 ± 3.7	5.3 ± 1.4	84.1 ± 8.2
MS DREAM		9.8 ± 4.6	5.3 ± 6.5	7.1 ± 1.0	66.0 ± 18.7
3D AFI		11.2 ± 2	-0.4 ± 2.9	11 ± 1.6	58.6 ± 12.8
3D RF-Prep	2p	11.9 ± 1.4	-7.3 ± 1.2	9.4 ± 1.1	53.1 ± 9.2
	3p (abs)	16.0 ± 4.0	1.9 ± 1.9	15.8 ± 4.1	41.8 ± 16.5
	3p (cpx)	8.7 ± 2.4	-1.1 ± 1.5	8.5 ± 2.5	68.2 ± 12.7

Note: All values are reported in %. MS: multi-slice, 2p: two-parameter method; 3p: three-parameter method; m-sub: magnitude-subtraction; c-sub: complex-subtraction.

improved accuracy (RMSE: 2.4% vs. 5.3% in the brain, 4.2% vs. 7.4% in the breast, 8.7% vs. 9.8% in the abdomen; Table 1) while only taking half of the scan time (8.6 s vs. 17 s). Note that the DREAM method requires that fully relaxed longitudinal magnetizations are established prior to the STEAM preparation pulses for each slice. Its accuracy can be affected by the T_1 -induced saturation effect, which demands a long waiting time after the previous sequence (not counted in the 17 s scan time) and a long temporal delay between neighboring slices.^{44,45} 3D AFI method suffered higher errors (Table 1) and longer scan time (148 s) than all other methods. In addition, ringing artifacts were also observed in AFI-derived unfiltered B_1 maps.¹⁰

Acquiring an additional image with the saturation preparation has also been proposed for improving the quantification model of T_2 -prepared myocardial T_2 mapping using a balanced SSFP acquisition with linear ramp-up pulses and linear profile ordering.⁵⁴ In that study, the saturated image was to capture the T_1 relaxation effect by the imaging pulses before acquiring the center of the k-space. In contrast, our theory is based on the PSF analysis of this k-space filtering effect for the low-high profile ordering used in this study (although it also applies to the linear profile ordering). Furthermore, the myocardial T_2 mapping technique assumed that all saturated images were positive numbers thus only magnitude images were used for fitting,⁵⁴ while in the current study negative data

were observed at some pixels and complex subtraction was shown to be more successful for improving the quantification accuracy (Figures 2 and 7, Supporting Information Figures S3, S5, S7, S8, S9, Table 1).


Our study had several limitations. 2D DAM with a single-shot fast-spin-echo acquisition was chosen as the reference method. DAM is based on the transverse magnetization after two hard pulses (60° and 120° , 0.58 ms) and 3D RF-prep is based on the longitudinal magnetization after one hard pulse (60° , 0.29 ms). Their different sensitivity to B_0 off-resonance or chemical shift such as fat (Figure 4, Supporting Information Figures S3, S5) needs to be considered when comparing the two methods. B_0 maps were not acquired in this study, which could provide useful information when evaluating the performance of each B_1 mapping technique. Last, the saturation module might be further improved for more robustness to B_0 and B_1 inhomogeneities.^{23,55} Only a modest CS acceleration factor of 3 was used for all B_1 mapping techniques. For the RF prepared approach with a separate 3D acquisition, a higher CS acceleration factor or a stack-of-spiral GRE readout^{56,57} could be used to further reduce the acquisition time.

5 | CONCLUSIONS

The proposed 3D RF-prepared three-parameter method with complex-subtraction for B_1 mapping delivered consistently higher accuracy in brain, breast, and abdomen than the traditional two-parameter method, the three-parameter method with magnitude-subtraction, the multi-slice DREAM and the 3D AFI, and was close to the results of 2D or multi-slice SDAM, while only taking a fraction of time of these existing methods above. This technique needs to be evaluated in a larger group of subjects for further evaluation.

ORCID

Dan Zhu  <https://orcid.org/0000-0002-0940-1519>

Michael Schär  <https://orcid.org/0000-0002-7044-9941>

Qin Qin  <https://orcid.org/0000-0002-6432-2944>

REFERENCES

- Bernstein MA, Huston J, Ward HA. Imaging artifacts at 3.0T. *J Magn Reson Imaging*. 2006;24:735-746.
- Merkle EM, Dale BM. Abdominal MRI at 3.0 T: the basics revisited. *Am J Roentgenol*. 2006;186:1524-1532.
- Adriany G, Van de Moortele PF, Wiesinger F, et al. Transmit and receive transmission line arrays for 7 tesla parallel imaging. *Magn Reson Med*. 2005;53:434-445.
- Ullmann P, Junge S, Wick M, Seifert F, Ruhm W, Hennig J. Experimental analysis of parallel excitation using dedicated coil setups and simultaneous RF transmission on multiple channels. *Magn Reson Med*. 2005;54:994-1001.
- Setsompop K, Alagappan V, Gagoski B, et al. Slice-selective RF pulses for in vivo B(1)(+) inhomogeneity mitigation at 7 tesla using parallel RF excitation with a 16-element coil. *Magn Reson Med*. 2008;60:1422-1432.
- Willinek WA, Gieseke J, Kukuk GM, et al. Dual-source parallel radiofrequency excitation body MR imaging compared with standard MR imaging at 3.0 T: initial clinical experience. *Radiology*. 2010;256:966-975.
- Rudrapatna SU, Juchem C, Nixon TW, de Graaf RA. Dynamic multi-coil tailored excitation for transmit B-1 correction at 7 tesla. *Magn Reson Med*. 2016;76:83-93.
- Deoni SCL, Rutt BK, Peters TM. Rapid combined T1 and T2 mapping using gradient recalled acquisition in the steady state. *Magn Reson Med*. 2003;49:515-526.
- Yarnykh VL. Optimal radiofrequency and gradient spoiling for improved accuracy of T1 and B1 measurements using fast steady-state techniques. *Magn Reson Med*. 2010;63:1610-1626.
- Boudreau M, Tardif CL, Stikov N, Sled JG, Lee W, Pike GB. B1 mapping for bias-correction in quantitative T1 imaging of the brain at 3T using standard pulse sequences. *J Magn Reson Imaging*. 2017;46:1673-1682.
- Sled JG, Pike GB. Correction for B1 and B0 variations in quantitative T2 measurements using MRI. *Magn Reson Med*. 2000;43:589-593.
- Jansen JFA, Backes WH, Nicolay K, Kooi ME. H1 MR spectroscopy of the brain: absolute quantification of metabolites. *Radiology*. 2006;240:318-332.
- Alger JR. Quantitative proton magnetic resonance spectroscopy and spectroscopic imaging of the brain: a didactic review. *Top Magn Reson Imaging*. 2010;21:115-128.
- Lecocq A, Le Fur Y, Maudsley AA, et al. Whole-brain quantitative mapping of metabolites using short echo three-dimensional proton MRSI. *J Magn Reson Imaging*. 2015;42:280-289.
- Katscher U, Voigt T, Findekklee C, Vernickel P, Nehrke K, Dossel O. Determination of electric conductivity and local SAR via B1 mapping. *IEEE Trans Med Imaging*. 2009;28:1365-1374.
- Voigt T, Katscher U, Doessel O. Quantitative conductivity and permittivity imaging of the human brain using electric properties tomography. *Magn Reson Med*. 2011;66:456-466.
- Katscher U, Kim DH, Seo JK. Recent progress and future challenges in MR electric properties tomography. *Comput Math Methods Med*. 2013;2013:546562.
- Liu J, Wang Y, Katscher U, He B. Electrical properties tomography based on B1 maps in MRI: principles, applications, and challenges. *IEEE Trans Biomed Eng*. 2017;64:2515-2530.
- Leijssen R, Brink W, van den Berg C, Webb A, Remis R. Electrical properties tomography: a methodological review. *Diagnostics*. 2021;11:176.
- Zhang XT, Schmitter S, Van de Moortele PF, Liu JE, He B. From complex B1 mapping to local SAR estimation for human brain MR imaging using Multi-Channel transceiver coil at 7T. *IEEE Trans Med Imaging*. 2013;32:1058-1067.
- Collins CM, Li SZ, Smith MB. SAR and B1 field distributions in a heterogeneous human head model within a birdcage coil. *Magn Reson Med*. 1998;40:847-856.
- Katscher U, Findekklee C, Voigt T. B1-based specific energy absorption rate determination for nonquadrature radiofrequency excitation. *Magn Reson Med*. 2012;68:1911-1918.

23. Sung K, Nayak KS. Design and use of tailored hard-pulse trains for uniformed saturation of myocardium at 3 tesla. *Magn Reson Med.* 2008;60:997-1002.
24. Qin Q, Shin T, Schär M, Guo H, Chen H, Qiao Y. Velocity-selective magnetization-prepared non-contrast-enhanced cerebral MR angiography at 3 tesla: improved immunity to B0/B1 inhomogeneity. *Magn Reson Med.* 2016;75:1232-1241.
25. Qin Q, van Zijl PC. Velocity-selective-inversion prepared arterial spin labeling. *Magn Reson Med.* 2016;76:1136-1148.
26. Shin T, Qin Q, Park JY, Crawford RS, Rajagopalan S. Identification and reduction of image artifacts in non-contrast-enhanced velocity-selective peripheral angiography at 3T. *Magn Reson Med.* 2016;76:466-477.
27. Shin T, Qin Q. Characterization and suppression of stripe artifact in velocity-selective magnetization-prepared unenhanced MR angiography. *Magn Reson Med.* 2018;80:1997-2005.
28. Qin Q, Qu Y, Li W, et al. Cerebral blood volume mapping using Fourier-transform-based velocity-selective saturation pulse trains. *Magn Reson Med.* 2019;81:3544-3554.
29. Liu D, Xu F, Li W, van Zijl PC, Lin DD, Qin Q. Improved velocity-selective-inversion arterial spin labeling for cerebral blood flow mapping with 3D acquisition. *Magn Reson Med.* 2020;84:2512-2522.
30. Li W, Liu D, van Zijl PCM, Qin Q. Three-dimensional whole-brain mapping of cerebral blood volume and venous cerebral blood volume using Fourier transform-based velocity-selective pulse trains. *Magn Reson Med.* 2021;86:1420-1433.
31. Liu D, Li W, Xu F, Zhu D, Shin T, Qin Q. Ensuring both velocity and spatial responses robust to B0/B1+ field inhomogeneities for velocity-selective arterial spin labeling through dynamic phase-cycling. *Magn Reson Med.* 2021;85:2723-2734.
32. Zhu D, Li W, Liu D, et al. Non-contrast-enhanced abdominal MRA at 3 T using velocity-selective pulse trains. *Magn Reson Med.* 2020;84:1173-1183.
33. Xu F, Li WB, Liu DP, et al. A novel spectrally selective fat saturation pulse design with robustness to B0 and B1 inhomogeneities: a demonstration on 3D T1-weighted breast MRI at 3 T. *Magn Reson Imaging.* 2021;75:156-161.
34. Akoka S, Franconi F, Seguin F, Le Pape A. Radiofrequency map of an NMR coil by imaging. *Magn Reson Imaging.* 1993;11:437-441.
35. Insko EK, Bolinger L. Mapping of the radiofrequency field. *J Magn Reson Ser A.* 1993;103:82-85.
36. Stollberger R, Wach P. Imaging of the active B1 field in vivo. *Magn Reson Med.* 1996;35:246-251.
37. Wang J, Qiu M, Constable RT. In vivo method for correcting transmit/receive nonuniformities with phased array coils. *Magn Reson Med.* 2005;53:666-674.
38. Wang J, Qiu M, Yang QX, Smith MB, Constable RT. Measurement and correction of transmitter and receiver induced nonuniformities in vivo. *Magn Reson Med.* 2005;53:408-417.
39. Wang J, Mao W, Qiu M, Smith MB, Constable RT. Factors influencing flip angle mapping in MRI: RF pulse shape, slice-select gradients, off-resonance excitation, and B0 inhomogeneities. *Magn Reson Med.* 2006;56:463-468.
40. Cunningham CH, Pauly JM, Nayak KS. Saturated double-angle method for rapid B1+ mapping. *Magn Reson Med.* 2006;55:1326-1333.
41. Sung K, Nayak KS. Measurement and characterization of RF nonuniformity over the heart at 3T using body coil transmission. *J Magn Reson Imaging.* 2008;27:643-648.
42. Yarnykh VL. Actual flip-angle imaging in the pulsed steady state: a method for rapid three-dimensional mapping of the transmitted radiofrequency field. *Magn Reson Med.* 2007;57:192-200.
43. Sacolick LI, Wiesinger F, Hancu I, Vogel MW. B1 mapping by Bloch-Siegert shift. *Magn Reson Med.* 2010;63:1315-1322.
44. Nehrke K, Bornert P. DREAM-a novel approach for robust, ultrafast, multi-slice B1 mapping. *Magn Reson Med.* 2012;68:1517-1526.
45. Nehrke K, Versluis MJ, Webb A, Bornert P. Volumetric B1+ mapping of the brain at 7T using DREAM. *Magn Reson Med.* 2014;71:246-256.
46. Hooijmans MT, Dzyubachyk O, Nehrke K, et al. Fast multistation water/fat imaging at 3T using DREAM-based RF shimming. *J Magn Reson Imaging.* 2015;42:217-223.
47. Nehrke K, Sprinkart AM, Bornert P. An in vivo comparison of the DREAM sequence with current RF shim technology. *Magma.* 2015;28:185-194.
48. Klose U. Mapping of the radio frequency magnetic field with a MR snapshot FLASH technique. *Med Phys.* 1992;19:1099-1104.
49. Chung S, Kim D, Breton E, Axel L. Rapid B1+ mapping using a preconditioning RF pulse with TurboFLASH readout. *Magn Reson Med.* 2010;64:439-446.
50. Breton E, McGorty K, Wiggins GC, Axel L, Kim D. Image-guided radio-frequency gain calibration for high-field MRI. *NMR Biomed.* 2010;23:368-374.
51. Zhu D, Qin Q. A revisit of the k-space filtering effects of magnetization-prepared 3D FLASH and balanced SSFP acquisitions: analytical characterization of the point spread functions. *Magn Reson Imaging.* 2022;88:76-88.
52. Ogg RJ, Kingsley PB, Taylor JS. WET, a T1- and B1-insensitive water-suppression method for in vivo localized 1H NMR spectroscopy. *J Magn Reson B.* 1994;104:1-10.
53. Rahbar H, Partridge SC, DeMartini WB, Gutierrez RL, Parsian S, Lehman CD. Improved B1 homogeneity of 3 tesla breast MRI using dual-source parallel radiofrequency excitation. *J Magn Reson Imaging.* 2012;35:1222-1226.
54. Akcakaya M, Basha TA, Weingartner S, Roujol S, Berg S, Nezafat R. Improved quantitative myocardial T2 mapping: impact of the fitting model. *Magn Reson Med.* 2015;74:93-105.
55. Golay X, Petersen ET, Hui F. Pulsed star labeling of arterial regions (PULSAR): a robust regional perfusion technique for high field imaging. *Magn Reson Med.* 2005;53:15-21.
56. Nielsen JF, Hernandez-Garcia L. Functional perfusion imaging using pseudocontinuous arterial spin labeling with low-flip-angle segmented 3D spiral readouts. *Magn Reson Med.* 2013;69:382-390.
57. Zi R, Zhu D, Qin Q. Quantitative T2 mapping using accelerated 3D stack-of-spiral gradient echo readout. *Magn Reson Imaging.* 2020;73:138-147.

SUPPORTING INFORMATION

Additional supporting information may be found in the online version of the article at the publisher's website.

Figure S1. The brain B_1^+ maps of one axial slice calculated from 2D DAM, 2D SDAM, multi-slice (MS) SDAM, MS DREAM, 3D AFI, and the 3D RF-prepared three-parameter method with complex-subtraction using [25, 50, 100, 225, 450] k-lines per shot with 3D FLASH acquisition and saturation delays of [0.5, 1.0, 3.0] s. The total scan time for each method is labeled at each top left corner.

Figure S2. Evaluating the performance of the 3D RF-prepared three-parameter method with complex subtraction using different numbers of k-lines per shot with 3D FLASH acquisition and various saturation delays, the mean and standard deviation of root mean square error (RMSE) values of each resulting B_1^+ maps compared with the 2D DAM in axial, coronal, and sagittal orientations for each of the three brains are compared. It can be observed that the protocol with a single-shot acquisition (450 k-lines per shot) and a 2.0 s saturation delay (the orange bar) produced a good balance between B_1^+ mapping accuracy (RMSE = $2.4 \pm 0.2\%$) and the scan time (8.6 s).

Figure S3. Evaluating the 3D RF-prepared B_1^+ mapping technique in the breast under fixed, adaptive, and SMART shims, respectively. For each shim condition, (top): the FA-encoded, the normalizing, and the saturated images, with the tissue masks labeled in solid red lines; (middle): the calculated B_1^+ maps using the 2D DAM method, the 3D RF-prepared two-parameter method, and the three-parameter method with both magnitude- and complex-subtractions; (bottom): their corresponding error maps (RF-prepared - DAM) with the averaged RMSE (root mean square error) indicated at the top right corners. FA: FA-encoded; norm: normalizing; sat: saturated; 2p: two-parameter method; 3p: three-parameter method; m-sub: magnitude-subtraction; c-sub: complex-subtraction.

Figure S4. The breast B_1^+ maps of one axial slice under fixed, adaptive, and SMART shims, respectively, calculated from 2D DAM, 2D SDAM, multi-slice (MS) SDAM, MS DREAM, 3D AFI, and the 3D RF-prepared three-parameter method with complex-subtraction.

Figure S5. Evaluating the 3D RF-prepared B_1^+ mapping technique in the abdomen under fixed and adaptive shims, respectively. For each shim condition, (top): the FA-encoded, the normalizing, and the saturated images, with the tissue masks labeled in solid red lines; (middle): the calculated B_1^+ maps using the 2D DAM method, the 3D RF-prepared two-parameter method, and the three-parameter method with both

magnitude- and complex-subtractions; (bottom): their corresponding error maps (RF-prepared - DAM) with the averaged RMSE (root mean square error) indicated at the top right corners. FA: FA-encoded; norm: normalizing; sat: saturated; 2p: two-parameter method; 3p: three-parameter method; m-sub: magnitude-subtraction; c-sub: complex-subtraction.

Figure S6. The abdomen B_1^+ maps of one axial slice under fixed, adaptive, and SMART shims, respectively, calculated from 2D SDAM, MS SDAM, MS DREAM, 3D AFI, and the 3D RF-prepared three-parameter method with complex-subtraction.

Figure S7. The swarm plot of the error mean values of different B_1^+ mapping methods compared to 2D DAM or SDAM methods grouping three orientations for each of the three brains, three shimming conditions for each of three breasts, two shimming conditions for each of the five abdomens. Across three organs, error mean of the 3D RF-prepared three-parameter (3p) method with complex-subtraction (c-sub) are consistently lower than the results of the two-parameter (2p) method or the 3p method with magnitude-subtraction (m-sub); error mean of the 3D RF-prepared 3p method with c-sub are consistently lower than the results of MS DREAM and are close to the results of 2D or MS SDAM for all three organs, and are consistently lower than the results of 3D AFI in the brain and breast and are lower or close to in the abdomen.

Figure S8. The swarm plot of the error standard deviation (SD) values of different B_1^+ mapping methods compared to 2D DAM or SDAM methods grouping three orientations for each of the three brains, three shimming conditions for each of three breasts, two shimming conditions for each of the five abdomens. Across three organs, error SD of the 3D RF-prepared three-parameter (3p) method with complex-subtraction (c-sub) are consistently lower than the results of the two-parameter (2p) method or the 3p method with magnitude-subtraction (m-sub); error SD of the 3D RF-prepared 3p method with c-sub are consistently lower than the results of 3D AFI and are close to the results of MS DREAM and 2D or MS SDAM for all three organs.

Figure S9. The swarm plot of the concordance correlation coefficient (CCC) values of different B_1^+ mapping methods compared to 2D DAM or SDAM methods grouping three orientations for each of the three brains, three shimming conditions for each of three breasts, two shimming conditions for each of the five abdomens. Across three organs, CCC of the 3D RF-prepared three-parameter (3p) method with complex-subtraction (c-sub) are consistently higher than the results of the two-parameter (2p) method or the 3p method with magnitude-subtraction (m-sub);

CCC of the 3D RF-prepared 3p method with c-sub are largely higher than the results of 3D AFI and are close to the results of 2D or MS SDAM for all three organs, and are consistently higher than the results of MS DREAM in the brain and breast and are close to in the abdomen.

How to cite this article: Zhu D, Schär M, Qin Q. Ultrafast B1 mapping with RF-prepared 3D FLASH acquisition: Correcting the bias due to T₁-induced k-space filtering effect. *Magn Reson Med*. 2022;88:757-769. doi: 10.1002/mrm.29247